



Publication Year	2016
Acceptance in OA@INAF	2020-05-05T13:51:37Z
Title	New Suns in the Cosmos II: differential rotation in Kepler Sun-like stars
Authors	Das Chagas, M. L.; Bravo, J. P.; Costa, A. D.; Ferreira Lopes, C. E.; Silva Sobrinho, R.; et al.
DOI	10.1093/mnras/stw2026
Handle	http://hdl.handle.net/20.500.12386/24511
Journal	MONTHLY NOTICES OF THE ROYAL ASTRONOMICAL SOCIETY
Number	463

New Suns in the Cosmos II: differential rotation in *Kepler* Sun-like stars

M. L. Das Chagas,^{1,2} J. P. Bravo,¹ A. D. Costa,¹ C. E. Ferreira Lopes,³
R. Silva Sobrinho,¹ F. Paz-Chinchón,^{4,5} I. C. Leão,⁶ A. Valio,⁷ D. B. de Freitas,¹
B. L. Canto Martins,¹ A. F. Lanza⁸ and J. R. De Medeiros^{1★}

¹Departamento de Física Teórica e Experimental, Universidade Federal do Rio Grande do Norte, Natal, RN 59078-970, Brazil

²Faculdade de Física – Instituto de Ciências Exatas, Universidade Federal do Sul e Sudeste do Pará, Marabá, PA 68505-080, Brazil

³SUPA Wide-Field Astronomy Unit, Institute for Astronomy, School of Physics and Astronomy, University of Edinburgh,

Royal Observatory, Blackford Hill, Edinburgh EH9 3HJ, UK

⁴Departamento de Enseñanza de las Ciencias Básicas, Universidad Católica del Norte, Larrondo 1281, Coquimbo 17814-21, Chile

⁵Millennium Institute of Astrophysics, Av. Vicuña Mackenna 4860, Macul, Santiago 78204-36, Chile

⁶European Southern Observatory, Karl-Schwarzschild-Strasse 2, Garching D-85748, Germany

⁷CRAAM, Universidade Presbiteriana Mackenzie, Rua da Consolação 896, São Paulo, SP 01302, Brazil

⁸INAF, Osservatorio Astrofisico di Catania, via S. Sofia 78, Catania I-95123, Italy

Accepted 2016 August 10. Received 2016 August 8; in original form 2016 April 5

ABSTRACT

The present study reports the discovery of Sun-like stars, namely main-sequence stars with T_{eff} , $\log g$ and rotation periods P_{rot} similar to solar values, presenting evidence of surface differential rotation (DR). An autocorrelation of the time series was used to select stars presenting photometric signal stability from a sample of 881 stars with light curves collected by the *Kepler* space-borne telescope, in which we have identified 17 stars with stable signals. A simple two-spot model together with a Bayesian information criterion were applied to these stars in the search for indications of DR; in addition, for all 17 stars, it was possible to compute the spot rotation period P , the mean values of the individual spot rotation periods and their respective colatitudes, and the relative amplitude of the DR.

Key words: stars: rotation – stars: solar-type – starspots.

1 INTRODUCTION

Stars are normally born with rapid rotation, and the angular velocity distribution will be established in their infancy stages, mostly as the result of the interaction of the stellar magnetic field with the circumstellar accretion disc, at least for late-type stars (e.g. Shu et al. 1994; Bouvier, Forestini & Allain 1997; van Saders & Pinsonneault 2013). During the initial stages, the surfaces of stars with convective envelopes will slow down via magnetic braking resulting from the interaction between the stellar magnetic field and the magnetized wind from the surface (e.g. Kawaler 1988; Reiners & Mohanty 2012).

Surface rotation can now be measured for many families of stars using different procedures, including the analyses of spectral line broadening, which produces projected rotational velocity $v \sin(i)$ measurements (e.g. De Medeiros & Udry 1999; Nordström et al. 2004; De Medeiros et al. 2014), and periodic modulation of starlight produced by non-uniformities on the surface of the stars (e.g. Affer et al. 2012; De Medeiros et al. 2013; McQuillan, Mazeh & Aigrain 2014; Leão et al. 2015). Other procedures include those based on

line core variations in the Ca II H and K lines (e.g. Baliunas et al. 1983) and on the Rossiter–McLaughlin effect or ellipsoidal light variations in eclipsing binaries.

In addition, it is now well established that the surface and internal stellar rotation pattern is by no means uniform. For instance, Helioseismology has revealed a large spread of rotation rates in the outer convective regions at different latitudes, with the inner regions presenting an almost constant rotation rate (e.g. Aerts et al. 2010). These aspects are intimately associated with the stellar differential rotation (hereafter DR), i.e. the property that different parts of the star rotate at different rates (Miesch 2005; Miesch & Toomre 2009; Kitchatinov 2013). The current leading theoretical basis, first presented by Lebedinsky (1941), explains DR based on the interaction between convection and rotation, with convective motions in a rotating star being disturbed by the Coriolis force. Its back reaction redistributes angular momentum and disturbs the global rotation behaviour to produce non-uniformities, leading to DR of the surface.

Different procedures can be used in the diagnosis of surface DR. In the first procedure, Doppler imaging, the positions of individual spots are estimated based on their effects on the stellar spectral line profiles, and on the condition that the star is rotating rapidly enough (e.g. Collier Cameron, Donati & Semel 2002). In the second

★ E-mail: renan@dfe.ufrn.br

procedure, the Fourier transform method, the Doppler shift at different latitudes due to rotation can be estimated from the Fourier transform of the line profiles (e.g. Reiners & Schmitt 2003; Reinhold & Reiners 2013). In the third procedure, time series photometry, the rotation periods can be computed from a time series of photometric observations (e.g. Lanza, Das Chagas & De Medeiros 2014; Aigrain et al. 2015; Davenport, Hebb & Hawley 2015). Another approach is based on asteroseismology, in which the frequency splitting of global oscillations is explained in terms of different latitudinal rotation rates (e.g. Gizon & Solanki 2004). A recent blind survey of competing techniques for detecting rotation and DR from model photometry, conducted by Aigrain et al. (2015), showed excellent agreement in recovering the overall rotation periods for stars exhibiting low and moderate activity levels. However, the referred study revealed a complex degeneracy between DR shear, spot lifetimes and the number of spots present, suggesting that DR studies based on full-disc light curves alone need to be treated with caution.

The advent of the space-borne *CoRoT* (Baglin et al. 2006) and *Kepler* (Borucki et al. 2010) telescopes made it possible to study in great detail the behaviour of the rotation of Sun-like stars. In this context, a large effort is being directed at the analysis of more active stars using the photometric modulations observed from their light curve (e.g. Bonomo & Lanza 2012; Fröhlich et al. 2012; De Medeiros et al. 2013; McQuillan, Aigrain & Mazeh 2013), therein producing rotation periods for thousands of different families of stars. A parallel effort is being made by different authors to enlarge the horizons of our quantitative and qualitative understanding of DR (e.g. Reinhold & Reiners 2013; Reinhold, Reiners & Basri 2013; Lanza et al. 2014; Aigrain et al. 2015; Reinhold & Gizon 2015).

Most of the DR surface patterns observed to date are predominantly solar type, with rotation rates decreasing from the equatorial to polar regions (e.g. Baliunas et al. 1983; Lanza, Rodono & Zappala 1993; Collier Cameron et al. 2002; Reiners & Schmitt 2003; Reinhold & Reiners 2013; Lanza et al. 2014). The DR total surface gradient varies to a high degree with the effective temperature (Barnes et al. 2005) and to a low degree with the rotation rate (Küker & Rüdiger 2005). Antisolar DR measurements are sparse and have mainly been performed for some late-type giant stars, most of which being components of RS Canum Venaticorum-systems (e.g. Strassmeier, Kratzwald & Weber 2003; Oláh, Jurcsik & Strassmeier 2003; Weber, Strassmeier & Washuettl 2005; Vida et al. 2007). As noted by different authors (e.g. Kovári et al. 2015), it appears that the strength and even the orientation of the DR are influenced by close companions, although such a scenario is not yet understood.

By applying asteroseismology procedures to time series obtained from light curve (hereafter LC) data from the *Kepler* or *CoRoT* missions, we are now in a position to extract, in addition to information about the surface rotational pattern, the physical characteristics of the stellar interior, revealing not only relevant aspects of DR but also information about pulsation modes and important constraints for dynamo models of low-mass stars. This enables one to test theoretical models for internal DR (see, e.g. Kitchatinov & Olemskoy 2011; Küker & Rüdiger 2011a), as well as the development of 3D simulations (e.g. Brun 2004; Browning 2008; Käpylä, Mantere & Brandenburg 2012). Further, it has been possible to estimate the ratio between the rotation rate in the small helium core and the large convective regions of late-type stars (e.g. Eggenberger et al. 2010).

This is the second paper of a series of studies devoted to the identification of Sun-like stars presenting physical properties similar to the Sun. In the first study (De Freitas et al. 2013), we identified stars representing potentially good matches to the Sun's rotation.

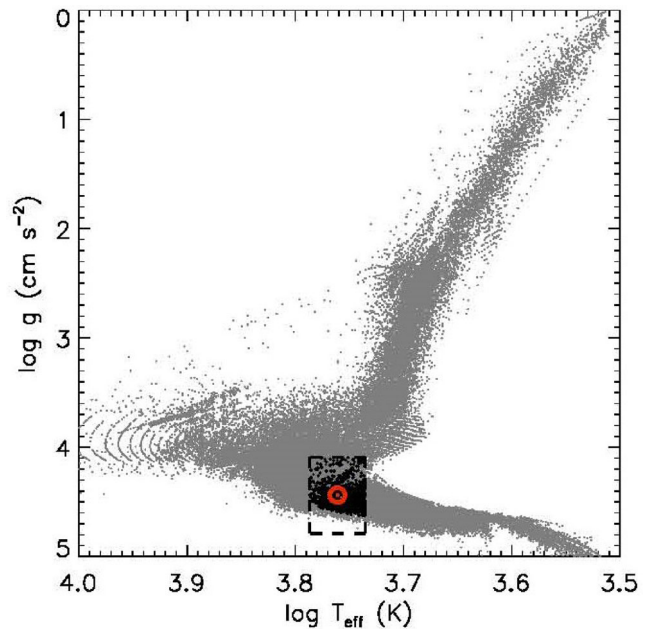


Figure 1. Distribution of $\log g$ and T_{eff} from entire *Kepler* data base. The black rectangle denotes the region of sources with solar parameters with T_{eff}^{\odot} and $\log g^{\odot}$. The red circle shows the position of the Sun, and the small black cross the stars of the sample analyzed.

The main goal of this work is to apply spot modelling (Lanza et al. 2014) for a large sample of Sun-like stars observed in the scope of the *Kepler* mission, therein attempting to measure DR and quantify how common DR is among Sun-like stars presenting solar parameters and, in particular, stars with similar Sun rotation periods. This paper is organized as follows: Section 2 presents the stellar sample with the *Kepler* stellar parameters. In Section 3, we introduce the autocorrelation function (ACF). Results and Conclusions are presented in Sections 4 and 5, respectively.

2 WORKING SAMPLE AND DATA ANALYSES

From 2009 May to 2013 May, the *Kepler* mission collected data in a steady field of view for 191 449 stars in 17 runs (known as quarters), which were composed of long-cadence (6.02 s observations stacked every 29.4 min; Jenkins et al. 2010) and short-cadence (bins of 59 s) observations (Van Cleve et al. 2010; Thompson et al. 2013). For this study, we selected the calibrated LCs processed by the PDC_MAP pipeline (Jenkins et al. 2010). To search for stars with physical properties approximately equal to the solar values, we made an initial selection of LCs from the *Kepler* data base (Mikulski Archive for Space Telescopes¹) using the solar parameters $\log g$ (~ 4.44) cm s^{-2} , T_{eff} (~ 5779) K, $[\text{Fe}/\text{H}]$ (~ 0) dex and $23 \text{ d} < P_{\text{rot}} < 33 \text{ d}$. A total of 881 stars with $3.94 \text{ cm s}^{-2} < \log g < 4.94 \text{ cm s}^{-2}$, $5579 \text{ K} < T_{\text{eff}} < 5979 \text{ K}$, were selected, with effective temperature and gravity obtained from Huber et al. (2014) and rotation period given by McQuillan et al. (2013). The location of our working sample, in the $\log g$ versus T_{eff} diagram, in the context of the entire *Kepler* stellar sample, is displayed in Fig. 1. With such a working sample at hand, a careful treatment was applied to the LCs, using the so-called co-trending basis vectors provided by the *Kepler* archive (see Twicken et al. 2010; Smith et al. 2012; Stumpe et al. 2012), to

¹ http://archive.stsci.edu/kepler/data_search/search.php, hereafter MAST

Table 1. Initial and final times of the intervals considered for the MCMC analysis, together with the BIC-computed values.

Star (KIC #)	t_1 (BKJD)	t_2 (BKJD)	BIC
2831979	1212.163	1255.382	4.097
4820062	735.384	761.804	18.778
5781991	131.513	164.984	5.300
5956717	1182.758	1207.585	8.027
6143158	411.224	439.158	17.008
6836955	261.205	293.591	10.65
7430659	863.035	899.592	3.261
8024188	1201.311	1240.893	7.467
8037792	634.978	676.926	16.325
8495770	844.746	880.383	19.635
9996105	264.290	336.132	3.183
10079452	448.517	499.623	8.413
10279927	1216.781	1239.504	18.279
10460082	416.803	442.203	11.926
10514649	205.096	247.352	4.528
11199277	1419.912	1465.927	14.378
12520213	820.143	869.328	7.102

remove systematic long-term trends originating from instruments, the environment, the detector or effects caused by the re-orientation of the spacecraft after each ~ 90 d. To remove outliers and prepare the LCs for the analysis using spot modelling, we applied the method developed by De Medeiros et al. (2013), a procedure that is able to identify discontinuities in the LCs, similar to that used by Basri et al. (2011). From this point on, an LC was considered to be fully treated, and its spot-modelling analysis could be performed.

3 THE AUTOCORRELATION METHOD

In this work, we follow the same procedure developed by Lanza et al. (2014) to estimate surface DR. First, we applied an ACF to check the stability of the photometric signal. Indeed, an important feature of the ACF is that it exhibits an oscillatory behaviour with

regularly spaced peaks; then, the coherence of a photometric signal can be estimated by the relative height of successive peaks in the ACF (Lanza et al. 2014). A crucial step in our analysis was the search for photometric signal stability for all 881 LCs constituting our initial working sample. From such analyses, we identified 17 stars presenting unambiguous stable photometric signals, indicating rotational modulation. Nevertheless, in spite of the fact that a significant DR can be detected when the relative height of the second maximum in the ACF is at least 0.6–0.7 (Lanza et al. 2014), we have considered a few stars whose ACF has a peak ratio smaller than this threshold because the Monte Carlo Markov chain (MCMC) analysis points for a significant DR for them. These stars with less good ACFs are flagged by a dagger in Table 2. Indeed, the ACF has been widely used in the study of photometric signals due to its ability to provide a good estimate of the average period variability, including stellar rotation period (e.g. Affer et al. 2012; McQuillan et al. 2013). Then, for these 17 stars with sufficiently stable signals, we applied spot modelling (Lanza et al. 2014) to seek individual spot rotation periods. The method of spot modelling is based on two spots and was applied with a Bayesian information criterion (hereafter BIC) to initially choose intervals of the time series presenting evidence of DR with starspots of almost constant areas. The initial and final times t_1 and t_2 , respectively, of those intervals are given in Table 1, together with the BIC-computed values for each of the 17 stars. Indeed, t_1 and t_2 are defined in Barycentric Kepler Julian Day (BKJD). Even if the time intervals are particularly small, the spot modelling is able to give us a valid signal of DR, as many other authors (e.g. Croll et al. 2006; Fröhlich 2007) have proven in previous studies. Readers are referred to Lanza et al. (2014) for a complete discussion of the ACF and the spot-modelling procedure. Nevertheless, let us underline an important aspect, previously considered by different authors (e.g. Jeffers & Keller 2009; Davenport et al. 2015), in the context of the present procedure. In the applied two-spot modelling, we cannot constrain the total number of starspots on the stellar surface, which, as noted by Davenport et al. (2015), may reflect two groups of spots or even many small spots across the entire stellar surface.

The LCs and the oscillatory behaviour of the ACF for these 17 stars are shown in Fig. A1 of Appendix. The blue vertical solid

Table 2. The stellar parameters and the results of MCMC analysis for our sample of 17 stars with traces of DR.

Star (KIC #)	P_{rot} (d)	$\log g$ (cm s^{-2})	T_{eff} (K)	P_1 (d)	σP_1 (d)	P_2 (d)	σP_2 (d)	$\Delta P/P$	$\sigma \Delta P/P$	$\Delta \Omega$ (d)
2831979*	24.383	4.363	5783	24.433	9.597×10^{-4}	22.660	1.629×10^{-3}	0.0753	8.332×10^{-5}	0.020 12
4820062*	23.098	4.104	5699	22.634	1.296×10^{-3}	24.771	2.676×10^{-3}	0.0886	1.347×10^{-4}	0.023 95
5781991†	31.464	4.466	5796	28.947	3.150×10^{-2}	33.006	4.909×10^{-2}	0.1310	2.007×10^{-3}	0.026 69
5956717*	23.297	4.213	5657	24.069	9.727×10^{-4}	21.828	6.862×10^{-4}	0.0976	5.440×10^{-5}	0.026 79
6143158†	23.155	4.509	5696	25.513	6.648×10^{-3}	21.448	2.218×10^{-3}	0.1731	3.243×10^{-4}	0.046 67
6836955†	26.354	4.61	5590	24.000	9.132×10^{-3}	26.724	5.223×10^{-3}	0.1074	4.371×10^{-4}	0.026 68
7430659*	28.388	4.268	5823	29.897	1.377×10^{-3}	26.440	2.351×10^{-3}	0.1227	1.027×10^{-4}	0.027 48
8024188*	23.849	4.384	5829	23.528	1.587×10^{-3}	22.754	1.653×10^{-3}	0.0334	1.007×10^{-4}	0.009 08
8037792*†	23.400	4.285	5666	24.797	3.245×10^{-3}	23.132	2.280×10^{-3}	0.0695	1.712×10^{-4}	0.018 23
8495770*†	25.634	4.545	5688	26.244	2.802×10^{-3}	25.832	1.605×10^{-3}	0.0158	1.250×10^{-4}	0.003 83
9996105	28.683	3.990	5815	30.006	1.936×10^{-2}	26.012	1.881×10^{-2}	0.1426	1.032×10^{-3}	0.032 15
10079452*	26.261	4.030	5812	25.092	7.177×10^{-3}	25.842	3.767×10^{-3}	0.0294	3.230×10^{-4}	0.007 26
10279927	24.018	4.508	5638	23.429	7.529×10^{-4}	22.373	8.778×10^{-4}	0.0461	5.166×10^{-5}	0.012 65
10460082*	26.027	4.554	5835	24.321	2.090×10^{-3}	28.001	3.333×10^{-3}	0.1407	1.610×10^{-4}	0.033 96
10514649*	24.205	4.388	5651	24.875	1.740×10^{-2}	22.694	1.084×10^{-2}	0.0917	9.016×10^{-4}	0.024 28
11199277*	29.339	4.493	5638	30.356	3.538×10^{-3}	28.019	1.479×10^{-3}	0.0801	1.366×10^{-4}	0.017 26
12520213	25.318	4.457	5679	25.270	3.361×10^{-3}	23.967	2.941×10^{-3}	0.0529	1.862×10^{-4}	0.013 52

*Stars with manifestation of DR, which are in common with Reinhold & Gizon (2015).

†Stars with ACFs lower than the threshold 0.6–0.7.

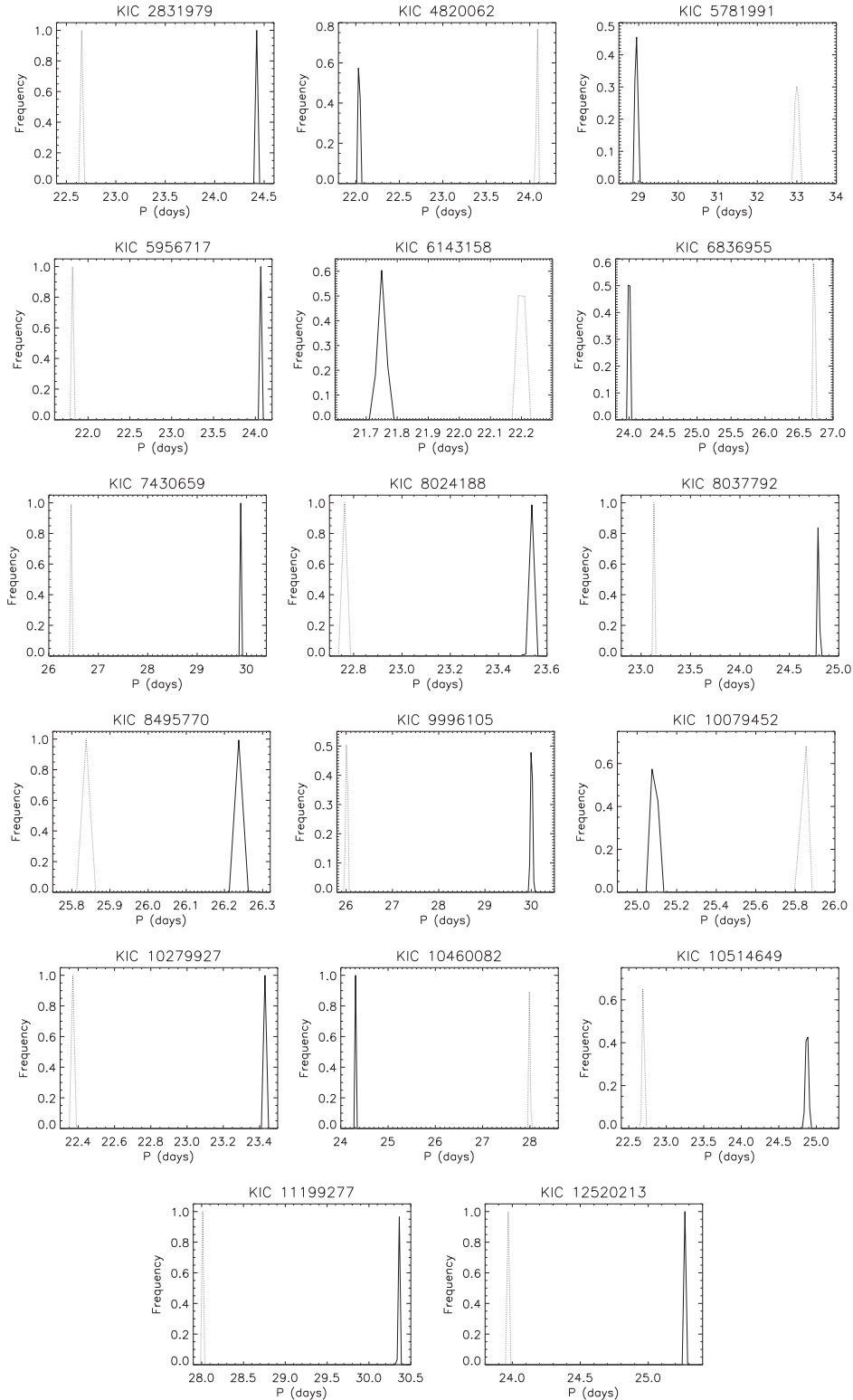


Figure 2. A posteriori distributions of the rotation periods of the two spots as derived from MCMC for all stars. The solid line refers to the distribution of the rotation period of the first spot, and the dashed line refers to that of the second.

lines display the initial and final times t_1 and t_2 of the intervals considered for the MCMC analysis. We then applied the procedure by Lanza et al. (2014) to compute the spot rotation period P , the mean values of the individual spot rotation periods P_1 and P_2 and their respective colatitudes, θ_1 and θ_2 , and the relative ampli-

tude of the DR, $\Delta P/P$, where $P = (P_1 + P_2)/2$. The a posteriori distributions of the rotation periods P_1 and P_2 of the two spots for all 17 stars, as derived from MCMC, are given in Fig. 2. The standard deviations of $\Delta P/P$ were also estimated by a model that assumes that starspots are not evolving along the fitted interval. Starspot

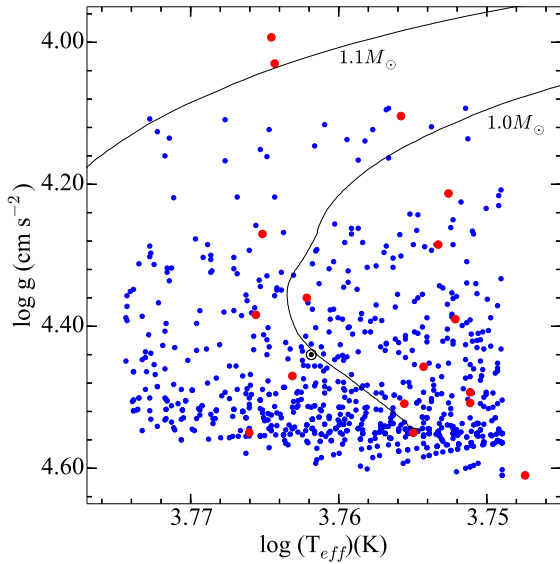


Figure 3. Distribution of Sun-like stars with measured DR in the $\log g$ and T_{eff} diagram, represented by red circles. Blue circles indicate stars of the original working sample without traces of DR. The evolutionary tracks are from Ekström et al. (2012). The Sun is represented by its usual symbol.

evolution can limit our accuracy in measuring DR at $\Delta\Omega \sim 1/t_{\text{evol}}$, where t_{evol} is the evolutionary time-scale, or even mimic a DR signal in the worst cases (see Aigrain et al. 2015).

4 RESULTS

The main results of the present study are given in Table 2, which lists the mean values of the individual spot rotation periods P_1 and P_2 , the relative amplitude of the DR lower limit, $\Delta P/P$ and the amplitude of the DR expressed as the frequency difference between the spots frequencies, $\Delta\Omega$. Table 2 lists also the stellar parameters P_{rot} , $\log g$ and T_{eff} . Fig. 3 displays, in the $\log g$ versus T_{eff} diagram, the locations of the 881 stars defined in our selection criteria, namely stars showing physical properties that are approximately equal to the Sun values, with $3.94 \text{ cm s}^{-2} < \log g < 4.94 \text{ cm s}^{-2}$, $5579 \text{ K} < T_{\text{eff}} < 5979 \text{ K}$, and the rotation period ranging into the solar values, from $23 \text{ d} < P_{\text{rot}} < 33 \text{ d}$. In the referred figure, the red points represent the 17 stars having spot lifetimes long enough for the detection of DR patterns on the basis of our spot-modelling method. Evolutionary tracks taken from Ekström et al. (2012) are overlaid to constrain the view of the mass range and evolutionary stage of the sample stars, with the position of the Sun indicated by the black symbol.

We compared the present results with Reinhold & Gizon (2015). Indeed, from our sample of 17 stars with measured amplitude of surface DR, 11 stars are found to be in common with those authors. For these common stars, Reinhold & Gizon (2015) detected the presence of multiple periods in their LCs, which were interpreted as the manifestation of DR, using a different approach based on the Lomb–Scargle periodogram. These stars are identified in Table 2 with an asterisk. A simple comparison between the DR values of this small sample of targets in common provides no correlation between the values, although they are distributed in a similar range. As a more robust test, we applied Student’s t -test, which can be used to compare whether measures in one sample are paired with measures in another sample. According to this method, the null hypothesis assumes that the true mean difference between the two observations

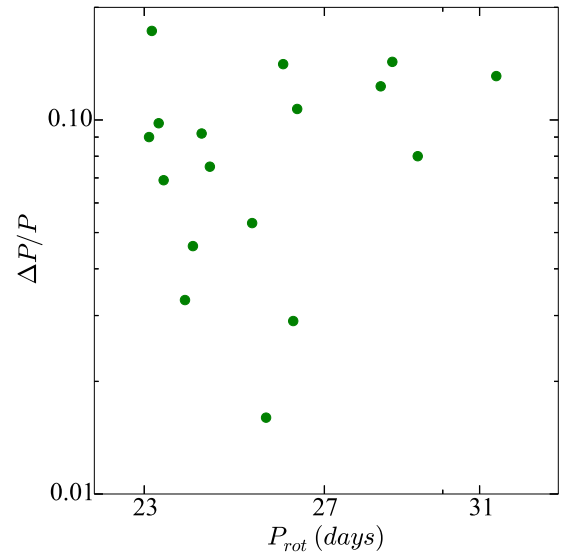


Figure 4. The distribution of the relative amplitude $\Delta P/P$ versus the rotation period P_{rot} for the 17 Sun-like stars with DR traces identified in the present study.

on each sample is zero; otherwise, the alternative hypothesis is considered. In this sense, the results of the paired t -test show that, because the $-t_{0.025}(-2.228) < t_{\text{computed}}(-0.959) < t_{0.025}(2.228)$ and because the p -value > 0.05 (confidence level), we cannot reject the null hypothesis. Such a fact may reflect, in principle, the difference in the nature of the procedures applied in the search for DR traces. In addition, the compatibility between their ranges suggests that their information is valid at least up to an order of magnitude.

Finally, we analysed the behaviour of the relative amplitude $\Delta P/P$ as a function of rotation period for our sample of 17 stars despite the narrow range of rotation periods considered in this study, namely, from 23 to 33 d. Fig. 4 displays the behaviour of P_{rot} versus $\Delta P/P$, from which one observes a soft trend of increasing $\Delta P/P$ towards longer rotation periods, paralleling the scenario found by different studies. For instance, as shown by Reinhold et al. (2013), the relative DR shear increases with longer rotation periods, in agreement with previous observations (Barnes et al. 2005) and theoretical approaches (Küker & Rüdiger 2011b).

5 CONCLUSIONS

Based on a simple two-spot model together with a BIC, we measured a lower limit on the amplitude of surface DR for 17 *Kepler* Sun-like stars. For these stars, using *Kepler* high-precision and evenly sampled photometric time series, it was possible to compute the spot rotation period P , the mean values of the individual spot rotation periods P_1 and P_2 and the relative amplitude of the DR, $\Delta P/P$, where $P = (P_1 + P_2)/2$. These stars present a soft trend of the estimated relative amplitude, $\Delta P/P$, increasing with increasing rotation periods, in agreement with the scenarios found in the literature, from several observational studies of DR, based on different measurement approaches.

In summary, although the art of measurements of the surface rotation of stars has now been mastered, with a high level of precision and maturity, the detection and measurement of stellar DR remains a tricky subject. In the present study, using a spot-modelling procedure, we were able to detect surface DR patterns in 17 stars with physical properties, including rotation, similar to the

Sun. The portrait emerging from this study points to a significant perspective: among Sun-like stars with surface rotation similar to the solar values, surface DR appears to be a common phenomenon.

ACKNOWLEDGEMENTS

The research activity of the Observational Astronomy Board of the Federal University of Rio Grande do Norte (UFRN) is supported by continuous grants from CNPq and FAPERN Brazilian agencies. We also acknowledge financial support from INCT INEspaço/CNPq/MCT. MLC, JPB and ADC acknowledge CAPES/PNPD fellowships. ICL and CEFL acknowledge CNPq/PDE fellowships. RSB and FPC acknowledge graduate fellowships from CAPES. DBdeF also acknowledges financial support by the Brazilian agency CNPq (Grant No. 306007/2015-0). This paper includes data collected by the *Kepler* mission. Funding for the *Kepler* mission is provided by the NASA Science Mission Directorate. All *Kepler* data presented in this paper were obtained from the Mikulski Archive for Space Telescopes (MAST). We would like to thank the anonymous referee for the helpful comments that lead us to a substantial improvement of this manuscript.

REFERENCES

- Aerts C. et al., 2010, *A&A*, 513, L11
 Affer L., Micela G., Favata F., Flaccomio E., 2012, *MNRAS*, 424, 11
 Aigrain S. et al., 2015, *MNRAS*, 450, 3211
 Baglin A., Auvergne M., Barge P., Deleuil M., Catala C., Michel E., Weiss W., COROT Team, 2006, in Fridlund M., Baglin A., Lochard J., Conroy L., eds, *ESA Special Publication Vol. 1306, Scientific Objectives for a Minisat: CoRoT*. ESA, Noordwijk, p. 33
 Baliunas S. L. et al., 1983, *ApJ*, 275, 752
 Barnes J. R., Collier Cameron A., Donati J.-F., James D. J., Marsden S. C., Petit P., 2005, *MNRAS*, 357, L1
 Basri G. et al., 2011, *AJ*, 141, 20
 Bonomo A. S., Lanza A. F., 2012, *A&A*, 547, A37
 Borucki W. J. et al., 2010, *Science*, 327, 977
 Bouvier J., Forestini M., Allain S., 1997, *A&A*, 326, 1023
 Browning M. K., 2008, *ApJ*, 676, 1262
 Brun A. S., 2004, in Danesy D., ed., *ESA Special Publication Vol. 559, SOHO 14 Helio- and Asteroseismology: Towards a Golden Future*. ESA, Noordwijk, p. 271
 Collier Cameron A., Donati J.-F., Semel M., 2002, *MNRAS*, 330, 699
 Croll B. et al., 2006, *ApJ*, 648, 607
 De Freitas D. B., Leão I. C., Ferreira Lopes C. E., Paz-Chinchon F., Canto Martins B. L., Alves S., De Medeiros J. R., Catelan M., 2013, *ApJ*, 773, L18
 De Medeiros J. R., Udry S., 1999, *A&A*, 346, 532
 De Medeiros J. R. et al., 2013, *A&A*, 555, A63
 De Medeiros J. R., Alves S., Udry S., Andersen J., Nordström B., Mayor M., 2014, *A&A*, 561, A126
 Davenport J. R. A., Hebb L., Hawley S. L., 2015, *ApJ*, 806, 212
 Eggenberger P. et al., 2010, *A&A*, 519, A116
 Ekström S. et al., 2012, *A&A*, 537, A146
 Fröhlich H.-E., 2007, *Astron. Nachr.*, 328, 1037
 Fröhlich H.-E., Frasca A., Catanzaro G., Bonanno A., Corsaro E., Molenda-Żakowicz J., Klutsch A., Montes D., 2012, *A&A*, 543, A146
 Gizon L., Solanki S. K., 2004, *Sol. Phys.*, 220, 169
 Huber D. et al., 2014, *ApJS*, 211, 2
 S. V., Keller C. U., 2009, in Stempels E., ed., *AIP Conf. Proc. Vol. 1094, Cool Stars, Stellar Systems and the Sun*. Am. Inst. Phys., New York, p. 664
 Jenkins J. M. et al., 2010, *ApJ*, 713, L87
 Käpylä P. J., Mantere M. J., Brandenburg A., 2012, *ApJ*, 755, L22
 Kawaler S. D., 1988, *ApJ*, 333, 236
 Kitchatinov L. L., 2013, in Kosovichev A. G., de Gouveia Dal Pino E., Yan Y., van Driel-Gesztelyi L., eds, *Proc. IAU Symp. 294, Solar and Astrophysical Dynamics and Magnetic Activity*. Cambridge Univ. Press, Cambridge, p. 399
 Kitchatinov L. L., Olemskoy S. V., 2011, *MNRAS*, 411, 1059
 Kovári Z. et al., 2015, *A&A*, 573, A98
 Küker M., Rüdiger G., 2005, *Astron. Nachr.*, 326, 265
 Küker M., Rüdiger G., 2011a, *Astron. Nachr.*, 332, 83
 Küker M., Rüdiger G., 2011b, *Astron. Nachr.*, 332, 933
 Lanza A. F., Rodono M., Zappala R. A., 1993, *A&A*, 269, 351
 Lanza A. F., Das Chagas M. L., De Medeiros J. R., 2014, *A&A*, 564, A50
 Leão I. C. et al., 2015, *A&A*, 582, A85
 Lebedinsky A. I., 1941, *Astron. Zh.*, 18, 10
 McQuillan A., Aigrain S., Mazeh T., 2013, *MNRAS*, 432, 1203
 McQuillan A., Mazeh T., Aigrain S., 2014, *ApJS*, 211, 24
 Miesch M. S., 2005, *Living Rev. Sol. Phys.*, 2, 1
 Miesch M. S., Toomre J., 2009, *Annu. Rev. Fluid Mech.*, 41, 317
 Nordström B. et al., 2004, *A&A*, 418, 989
 Oláh K., Jurcsik J., Strassmeier K. G., 2003, *A&A*, 410, 685
 Reiners A., Mohanty S., 2012, *ApJ*, 746, 43
 Reiners A., Schmitt J. H. M. M., 2003, *A&A*, 398, 647
 Reinhold T., Gizon L., 2015, *A&A*, 583, A65
 Reinhold T., Reiners A., 2013, *A&A*, 557, A11
 Reinhold T., Reiners A., Basri G., 2013, *A&A*, 560, A4
 Shu F., Najita J., Ostriker E., Wilkin F., Ruden S., Lizano S., 1994, *ApJ*, 429, 781
 Smith J. C. et al., 2012, *PASP*, 124, 1000
 Strassmeier K. G., Kratzwald L., Weber M., 2003, *A&A*, 408, 1103
 Stumpe M. C. et al., 2012, *PASP*, 124, 985
 Thompson M. A. et al., 2013, *PASP*, 125, 809
 Twicken J. D., Chandrasekaran H., Jenkins J. M., Gunter J. P., Girouard F., Klaus T. C., 2010, in Radziwill N. M., Bridger A., eds, *Proc. SPIE Conf. Ser. Vol. 7740, Software and Cyberinfrastructure for Astronomy*. SPIE, Bellingham, p. 1
 Van Cleve J. E. et al., 2010, *American Astronomical Society Meeting Abstracts*. p. 420.02
 van Saders J. L., Pinsonneault M. H., 2013, *ApJ*, 776, 67
 Vida K., Kovári Z., Švanda M., Oláh K., Strassmeier K. G., Bartus J., 2007, *Astron. Nachr.*, 328, 1078
 Weber M., Strassmeier K. G., Washuettl A., 2005, *Astron. Nachr.*, 326, 287

APPENDIX: FIGURES

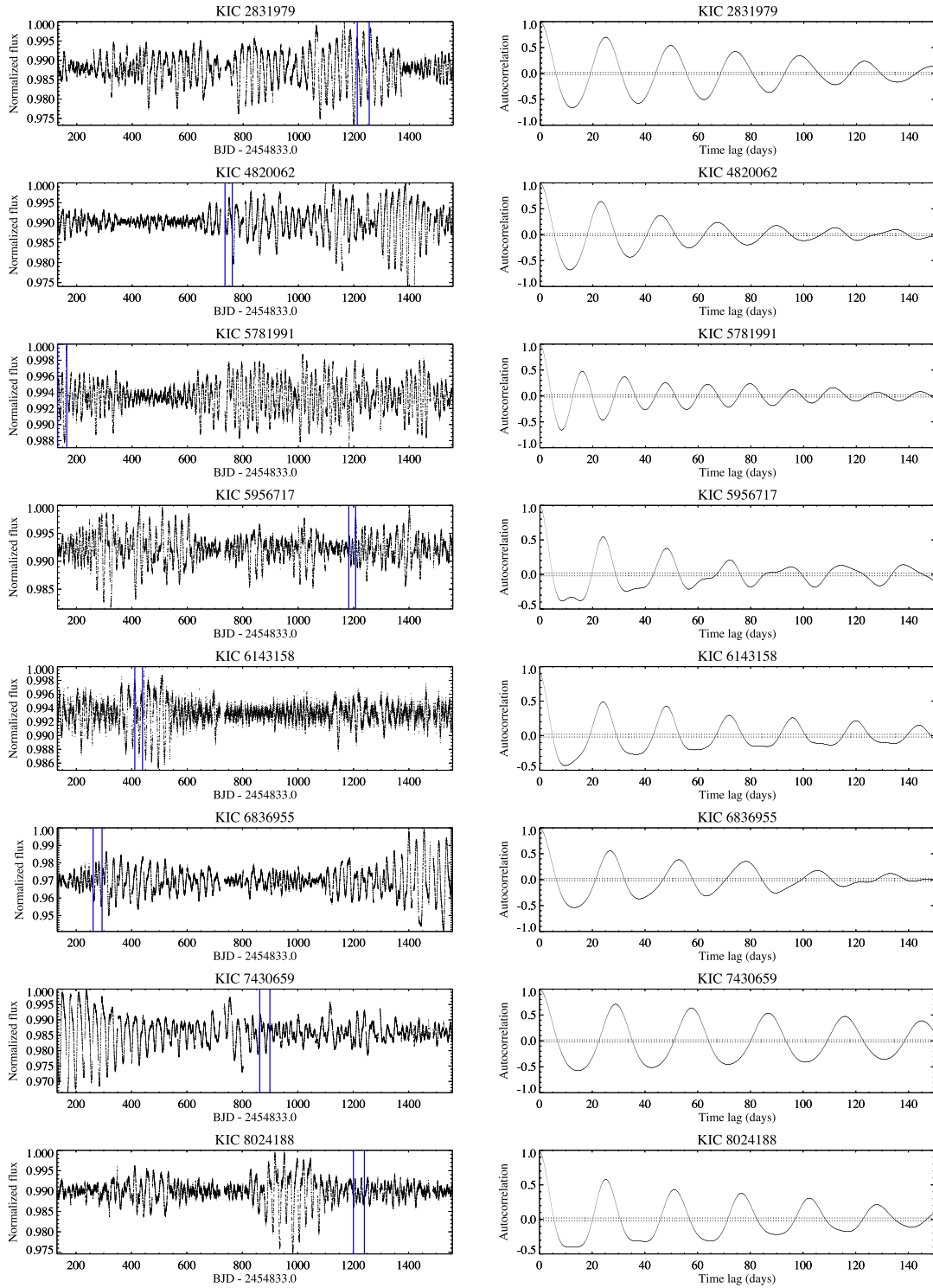


Figure A1. Left: photometric times series of *Kepler* stars (from top to bottom) KIC 2831979, KIC 4820062, KIC 5781991, KIC 5956717, KIC 6143158, KIC 6836955, KIC 7430659, KIC 8024188, KIC 8037792, KIC 8495770, KIC 9996105, KIC 10079452, KIC 10279927, KIC 10460082, KIC 10514649, KIC 11199277 and KIC 12520213. The flux has been normalized to the maximum value observed along each time series. The vertical solid lines (in blue) display the initial and final times of the intervals considered for MCMC analysis (see Table 1). Right: autocorrelation functions of the LCs of the stars in our sample. The dotted lines indicate the interval corresponding to $\pm\sigma$, where σ is one standard deviation of the autocorrelation as expected for a pure random noise with some degree of autocorrelation according to the large-lag approximation.

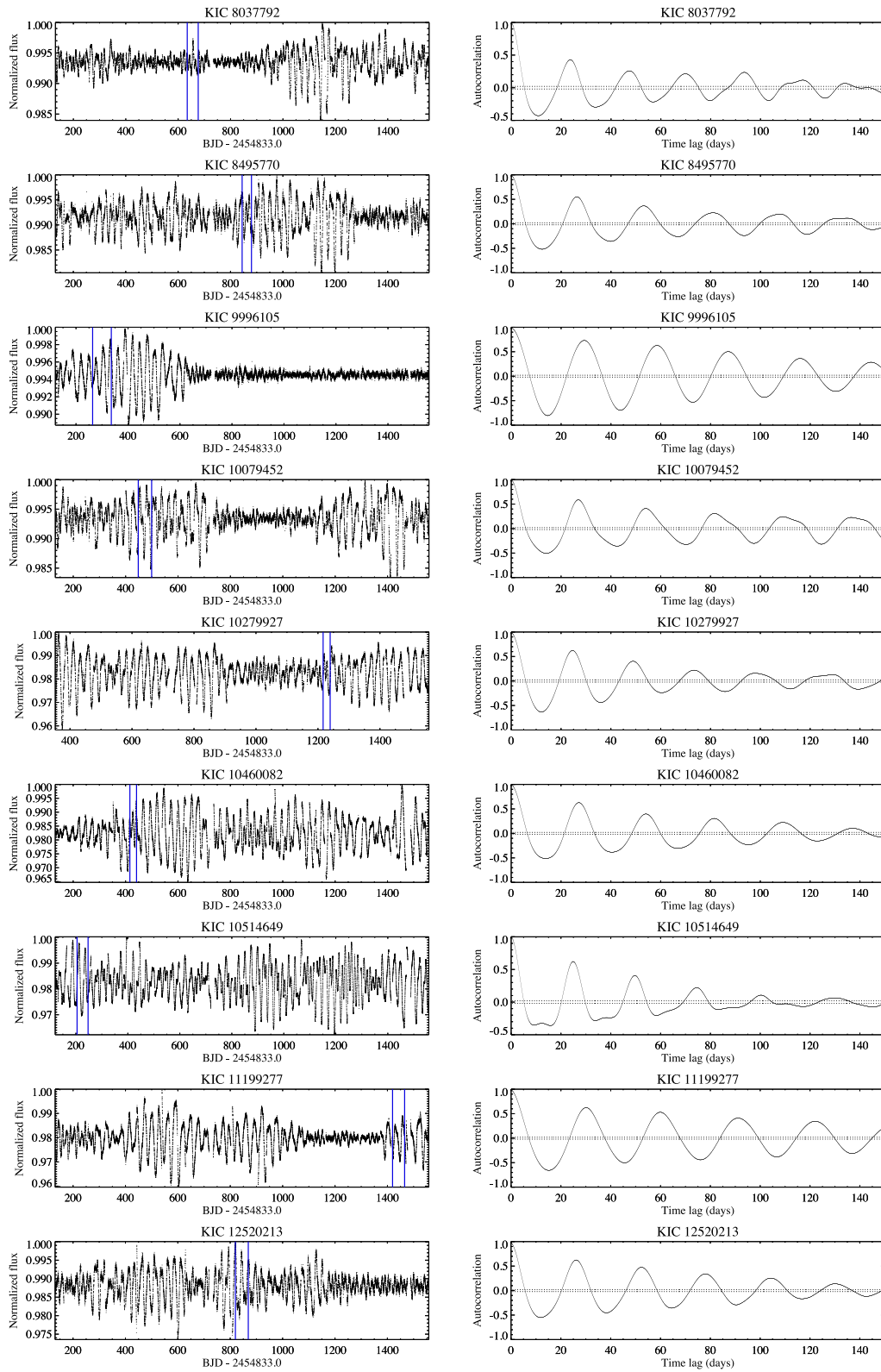


Figure A1 – continued

This paper has been typeset from a $\text{\TeX}/\text{\LaTeX}$ file prepared by the author.